Sensors and Materials, Vol. 35, No. 10 (2023) 4617–4632
MYU Tokyo

S & M 3418

Analysis of Chemical Composition Formula of Sealing Alloys Using Nearest-neighbor Two-shell Model

Hai-Lian Hong, Chi-Hsin Yang,* Hui-Xian Yan,
Lian-Hui Zheng, and Kun-Chieh Wang

School of Mechanical and Electric Engineering, Sanming University, Sanming 365004, Fujian Province, China

(Received July 14, 2023; accepted October 5, 2023)

Keywords: nearest-neighbor two-shell structure, Fe–Ni alloys, sealing alloys, structural model, composition analysis, Friedel spherical periodic resonance

The composition design of sealing alloys still inevitably relies on the trial-and-error method, leading to the unnecessary waste of time and materials. The main goal of this study is to introduce an electronic structure model, named the nearest-neighbor two-shell (NNTS) model, to guide the composition design of the face-centered cubic (fcc) solid solution alloy. The chemical structure formula of the model is $[X–Y_{12}]Z_2$, where X, Y, and Z are the composited atomics in the alloy. The atomic structure of the model is developed by comparing with the Friedel sphere periodic electronic resonance structure. We applied the proposed model to analyze various iron–nickel (Fe–Ni) binary and ternary alloys, and the obtained results were consistent with those calculated using the Cowley parameters. The discovery of the model is conducive to gaining a deeper understanding of the composition distribution of alloys and also provides a new way to design the alloy composition.

1. Introduction

Recently, various vacuum devices have been widely used in various fields, such as micro-electro-mechanical systems (MEMS),[1] solar vacuum tubes,[2] and vacuum glass.[3] To improve the strength, antipollution performance, and service life of the vacuum devices, it is necessary to apply some sealing techniques to construct a vacuum chamber. The technology consisting of sealing materials and sealing techniques is the core in the preparation of vacuum devices. For example, nanomaterial graphene with a single-atom thickness is used to achieve high sealing performance in MEMS,[4] glass is sealed with organic compounds at low sealing temperatures,[3] and various types of sealing glass with good chemical compatibility are sealed with tempered glass.[5] Because the metal sealing material has a low melting point and excellent corrosion and oxidation resistances, it is the preferred material for sealing glass. Indium alloy is used to seal glass edges at a low temperature of 220 °C,[6] silver paste is used to seal tempered glass at 450 °C for 10 min,[7] and aluminum and glass are reliably sealed at 400 °C using anodic bonding technology.[8]

*Corresponding author: e-mail: 20190207@fjsmu.edu.cn
https://doi.org/10.18494/SAM4581

ISSN 0914-4935

Iron–nickel (Fe–Ni) alloys have high strength, high thermal conductivity, and even no magnetism. Below the temperature of 500 ℃, the most outstanding advantage is that Fe–Ni alloys have a stable thermal-expansion coefficient that is very close to that of glass. Therefore, Fe–Ni alloys are the suitable sealing materials to be used with glass. However, the composition range of Fe–Ni sealing alloys is 42 to 54 wt.% nickel and is far from the 36 wt.% of the alloy with the lowest thermal-expansion coefficient. The selection rules for the nickel content in Fe–Ni alloys are not yet clearly indicated in the literature.

Excellent properties of alloys are governed by stable structures, which originate from short-range ordered structures.[9–13] Mechanical properties such as strength,[14] fracture toughness,[15] and the functional properties of expansion[16] and corrosion resistance[17] are all related to the short-range ordered structure of an alloy. Therefore, there are many studies on short-range ordered structures, especially the nearest-neighbor two-shell (NNTS) model, which will be proposed herein. For example, the average concentration,[18] spin wave,[19] and ordering transition temperature[20] are all evaluated by applying the NNTS model. The computed results are more consistent with the experimental values than those obtained by only applying the nearest-neighbor first-shell atomic model.

Motivated by the correlation between the NNTS structure and the properties of alloys, there is an urgent need to establish the NNTS model to analyze the composition of the alloys and then to achieve an effective method for designing the alloys. The novelty and contribution of this work are the development of the NNTS electronic structure model and the assignment of the chemical structural formula (CSF), so as to avoid unnecessary material waste and shorten the time duration for alloy design in the traditional alloy development.

The rest of this paper is organized as follows. In Sect. 2, the distribution of the first and second nearest-neighbor atoms is obtained by analyzing the three ordered phases of Fe–Ni alloys. Then, the probability distribution of the first and second neighbor atoms of Fe–Ni alloys is calculated by using the short-range ordered Cowley parameters. The composition of Fe–Ni alloys is analyzed using the ideal cluster or bi-cluster formula. In Sect. 3, the most stable short-range ordered structure model, the 2–2 model, is found by comparing the calculated models from the Friedel spherical periodic resonance structure. In Sect. 4, the compositions of commonly used Fe–Ni binary and ternary sealing alloys are analyzed using the 2–2 model. Finally, some concluding remarks are provided.

2. Determination of Nearest Two-shell Atomic Compositions

2.1 Nearest two-shell atomic distributions

Referring to the literature,[21] the phase diagram of Fe–Ni alloys is shown in Table 1. We have found that there are three ordered phases with highly stable structures, Fe_3Ni, FeNi, and $FeNi_3$, easily formed at low temperatures.[21] The two nearest-neighbor cluster formulas for the order phases of Fe–Ni alloys are analyzed below.

(1) In the ordered phase of $Fe_3Ni(L1_2)$, the first nearest neighbor centered on an Fe atom is composed of 12 nickel atoms and the second nearest neighbor is composed of six iron atoms.

Table 1
(Color online) Two nearest-neighbor cluster formulas for the ordered phase of Fe–Ni alloys.

Component Ni at.%*	Ordered phase	Centered around Ni atom (white sphere)		Centered around Fe atom (blue sphere)	
25	Fe_2Ni	$Ni–Ni_8Fe_4–Ni_6$	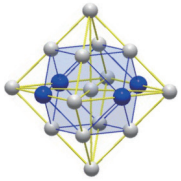	$Fe–Ni_{12}–Fe_6$	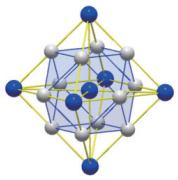
50	FeNi	$Ni–Fe_8Ni_4–Ni_6$	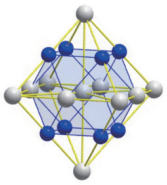	$Fe–Ni_8Fe_4–Fe_6$	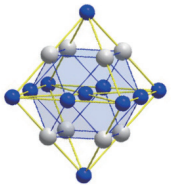
75	$FeNi_3$	$Ni–Fe_{12}–Ni_6$	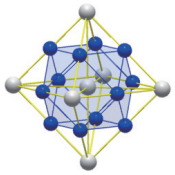	$Fe–Fe_8Ni_4–Fe_6$	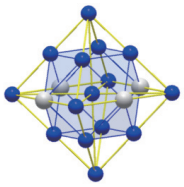

In the former case, the first neighbor is Ni_8Fe_4 and the second neighbor is composed of six Ni atoms.

(2) In the ordered phase of FeNi($L1_0$), the first neighbor centered on a Ni atom is Fe_8Ni_4, and the second neighbor is composed of six Ni atoms. Otherwise, the first neighbor centered on an Fe atom is Ni_8Fe_4 and the second neighbor is composed of six Fe atoms.

(3) In the ordered phase of $FeNi_3$($L1_2$), the positions of the nearest shell atoms are opposite to those of Fe and Ni atoms in the ordered phase of Fe_3Ni. That is, the Fe atoms are replaced by Ni atoms and Ni atoms are changed to Fe atoms in Fe_3Ni ($L1_2$).

Remark 1

In the face-centered cubic (fcc) lattice of the $L1_2$ structure, the face center is occupied by a type-A atom and the vertex is occupied by a type-B atom. The $L1_0$ structure comprises an alternating stack of atomic surfaces consisting of only A atoms and only B atoms along the [0 0 1] direction in the fcc lattice.[22]

Remark 2

In Table 1, at.% is the abbreviation for the atomic percentage of Ni in Fe–Ni alloys. Each of the three ordered phases of Fe–Ni alloys similarly show the property that the first shell tends to be composed of dissimilar atoms and the second shell tends to be composed of atoms of the same type in the central atom of the ordered phase. This means that the attraction between dissimilar atoms is greater than that between atoms of the same type. When dissimilar atoms are arranged as close neighbors to each other, an Fe–Ni alloy has the lowest energy and the most stable

structure owing to the strong binding force between the atoms. In Ref. 23, it is pointed out that the chemical short-range ordered structure is determined by the magnitude and sign of mixing enthalpy. When the sign of mixing enthalpy is negative, heterogeneous atoms tend to be close neighbors, and when the sign is positive, homogeneous atoms tend to be close neighbors.

As an example, in single-phase fcc Fe–Ni alloys, the mixing enthalpy of Fe–Ni alloys with a Ni content exceeding 25 at.% is $\Delta H_{\mathrm{Fe–Ni}} = 0$ to 9.6 KJ/mol.[23] The dissimilar atoms, Fe and Ni atoms, tend to be close to each other with a negative sign of mixing enthalpy. In this case, atoms of the same type, Fe and Fe or Ni and Ni atoms, appear as the second nearest atoms. Then, the attraction between dissimilar atoms in Fe–Ni alloys is greater than that between atoms of the same type. This is further proven later.

2.2 Ideal chemical composition formula (CCF) defined by Cowley parameters

The short-range ordered structure of solid solution alloys is characterized by Cowley parameters.[24] Assuming that two types of atom, type-U and type-V, are found in the solution of an alloy, the Cowley parameter is defined by $\alpha = 1 - P_U/X_U$, where P_U is the distributed probability of the type-U atom around the central type-V atom in the solid solution alloy and X_U is the molar fraction of the type-U atom. When $\alpha = 0$, the type-U and type-V atoms have a disorderly distribution. Otherwise, in the case of $\alpha < 0$, the type-U and type-V atoms are heterogeneous neighbors and are segregated neighbors in the case of $\alpha > 0$.[24]

The distribution of atoms in the two nearest shells for an Fe–Ni alloy can be calculated by applying the Cowley parameters. The typical sequence of procedures and results provided in Ref. 25 are summarized.

(1) For the $Fe_{46.5}Ni_{53.5}$ (at.%) alloy with the fcc single phase, the two sets of Cowley parameters are $\alpha_{110} = -0.07665$; $\alpha_{200} = 0.06463$ and $\alpha_{110} = -0.1396$; $\alpha_{200} = 0.10073$, which are obtained by neutron diffraction experiments and Monte Carlo simulations.[25]

(2) If the Ni atom is taken to be the central atom V, the mole fraction of U atoms (Fe atoms) is $X_U = 46.5\%$; then, the probability of Fe atoms being around the Ni atom is found to be $P_U = (1 - \alpha)X_U = (1 + 0.07665) * 46.5\% = 50\%$ by substituting $\alpha_{110} = -0.07665$. That is, the composition of the 12 nearest shell atoms is Fe_6Ni_6.

(3) By replacing $X_U = 46.5\%$ with $\alpha_{200} = 0.06463$, the probability of an Fe atom appearing in the second shell, which is centered on the Ni atom, is $P_U = (1 - \alpha)X_U = (1 - 0.06463) * 46.5\% = 43.5\%$. That is, the composition is $Fe_{0.87}Ni_{1.13}$ for the six atoms in the second shell. It is concluded that the nearest-neighbor shell atoms with Ni atom at the center are arranged as Ni–Fe_6Ni_6–$Fe_{0.87}Ni_{1.13}$, where only two effective atoms in the second shell participate in the electron cloud resonance of the central atom.

(4) Optimizing the formula of Ni–Fe_6Ni_6–$Fe_{0.87}Ni_{1.13}$ using the integer ratio of atoms, Ni–Fe_7Ni_5–Ni_2 is derived with the Ni atom at the center. Otherwise, if the Fe atom is taken as the center, the distribution of the nearest two-shell atoms becomes Fe–Ni_8Fe_4–Fe_2. The chemical composition of the alloy is 53.3 at.% Ni, which is basically consistent with the composition of the alloy, and the deviation is −0.2%. This means that the composition of the Fe–Ni alloy can be resolved by applying the model of atoms in the two nearest shells. The feasibility of this model has also been verified in another Fe–Ni alloy.

The feasibility of the aforementioned procedures has also been verified for various components for Fe–Ni alloys in previous work.[26–30] The evaluated results are shown in Table 2. As seen in Table 2, when the range of Ni contents is between 30.2 and 77.5 at.%, the 12 atoms in the first shell centered on Ni are distributed between $Fe_{8.58}Ni_{3.42}$ and $Fe_{3.01}Ni_{8.93}$ according to the results of evaluations using the Cowley parameters. Ideally, the atoms in the second shell and the central atom should be of the same type, Ni.

By adjusting all the atoms in the second shell as Ni atoms, the ideal CCF of all alloys is obtained. The deviation of the Ni component ratio from the alloy component is not more than 0.3%. However, in the ideal CCF of the shell, the drawback is that the alloy cannot be resolved using the integer formula, except for the alloy with 53.5 at.% Ni.

To mitigate the aforementioned drawback of the ideal CCF, each Fe–Ni alloy listed in Table 2 is further analyzed utilizing the double cluster model. The following key points are revealed in this work:

(1) When the content of Ni is 30.2 at.%, there are two types of nearest-neighbor shell cluster, namely, $[Ni–Ni_8Fe_4]$ with the central Ni atom and $[Fe–Fe_{12}]$ centered on an Fe atom. The two clusters originate from the ordered phase Fe_3Ni and the pure Fe atoms, respectively. Otherwise, the cluster form $[Ni–Ni_8Fe_4]Fe_2$ in this component does not satisfy the second nearest-neighbor order owing to the Fe-rich composition. There are not enough Ni atoms to form the second nearest-neighbor order with the central atom.
(2) When the content of Ni is 36.8 at.%, there are two types of nearest-neighbor shell cluster, $[Ni–Fe_8Ni_4]$ and $[Fe–Fe_8Ni_4]$, which originate from the ordered phases FeNi and $FeNi_3$. The second-shell atoms form the second nearest-neighbor order with the central Ni and Fe atoms, respectively. The double clusters are $[Ni–Fe_8Ni_4]Ni_2$ and $[Fe–Fe_8Ni_4]Fe_2$, respectively.
(3) When the content of Ni is 75–77.5 at.%, there are two types of nearest-neighbor shell cluster, $[Fe–Ni_8Fe_4]$ and $[Ni–Ni_{12}]$, which belong to the ordered phase FeNi and the pure Ni atoms. The second-shell atoms form the second nearest-neighbor order with the central Fe and Ni atoms, respectively. The double clusters are $[Fe–Ni_8Fe_4]Fe_2$ and $[Ni–Ni_{12}]Ni_2$, respectively.

According to the above discussion, it is concluded that the double cluster model with an integer ratio of Fe and Ni atoms is suitable for analyzing all of the real Fe–Ni alloys shown in Table 2. Furthermore, the analyzed results are also consistent with the results of calculations using the Cowley parameters of the various Fe–Ni alloys. In the double cluster model, the first nearest-neighbor atom arrangement is derived from three types of relatively stable ordered phase with the pure Fe, pure Ni, and Fe–Ni alloys. The second nearest neighbor and the central atom are basically of the same type, which satisfies the ideal atomic distribution. This is further proof that all of the Fe–Ni alloys can be resolved by the double cluster model with two atoms in the second nearest-neighbor shell. That is, 15 atoms in the range of the nearest-neighbor atoms are participating in the resonance.

In the fcc atomic lattice structure, there are 6 atoms in the second nearest neighbor. However, the resonance of the first nearest-neighbor cluster with stronger relative force can only drive two atoms in the second nearest neighbor to participate in the resonance. This is deduced from the spherical period theory as follows.

Table 2
Cluster formulas of Fe–Ni alloys.

Composition Ni at.%	Cowley parameters	Two nearest-neighbor CCF centered on Ni	Two nearest-neighbor CCF centered on Fe	Ideal CCF centered on Ni atoms	Ideal CCF centered on Fe atoms	Bi-cluster formula	Composition for bi-cluster formula	Deviation at.%
30.2[26]	$\alpha_{110} = -0.0201$ $\alpha_{200} = 0.0451$	Ni–$Fe_{8.51}Ni_{3.49}$–$Fe_{1.33}Ni_{0.67}$	Fe–$Ni_{8.51}Fe_{3.49}$–$Ni_{1.33}Fe_{0.67}$	$[Ni–Fe_{10.5}Ni_{1.5}]Ni_2$	$[Fe–Fe_{7.5}Ni_{4.5}]Fe_2$	$[Ni–Ni_8Fe_4]Fe_2$ + $[Fe–Fe_{12}]Fe_2$	30	–0.2
30.2[27]	$\alpha_{110} = -0.0282$ $\alpha_{200} = 0.0562$	Ni–$Fe_{8.58}Ni_{3.42}$–$Fe_{1.31}Ni_{0.69}$	Fe–$Ni_{8.58}Fe_{3.42}$–$Ni_{1.31}Fe_{0.69}$					
36.8[28]	$\alpha_{110} = -0.0583$ $\alpha_{200} = 0.0522$	Ni–$Fe_{8.03}Ni_{3.97}$–$Fe_{1.20}Ni_{0.80}$	Fe–$Ni_{8.03}Fe_{3.97}$–$Ni_{1.20}Fe_{0.80}$	$[Ni–Fe_{9.5}Ni_{2.5}]Ni_2$	$[Fe–Fe_{6.5}Ni_{5.5}]Fe_2$	$[Ni–Fe_8Ni_4]Ni_2$ + $[Fe–Fe_8Ni_4]Fe_2$	36.6	–0.2
36.8[27]	$\alpha_{110} = -0.0797$ $\alpha_{200} = 0.0675$	Ni–$Fe_{8.19}Ni_{3.81}$–$Fe_{1.18}Ni_{0.82}$	Fe–$Ni_{8.19}Fe_{3.81}$–$Ni_{1.18}Fe_{0.82}$					
53.5[25]	$\alpha_{110} = -0.07665$ $\alpha_{200} = 0.06463$	Ni–Fe_6Ni_6–$Fe_{0.87}Ni_{1.13}$	Fe–Ni_6Fe_6–$Ni_{0.87}Fe_{1.13}$	$[Ni–Fe_7Ni_5]Ni_2$	$[Fe–Ni_8Fe_4]Fe_2$	—	53.3	–0.2
53.5[27]	$\alpha_{110} = -0.1396$ $\alpha_{200} = 0.10073$	Ni–$Fe_{6.36}Ni_{5.64}$–$Fe_{0.84}Ni_{1.16}$	Fe–$Ni_{6.36}Fe_{5.64}$–$Ni_{0.84}Fe_{1.16}$					
75[30]	$\alpha_{110} = -0.111$ $\alpha_{200} = 0.136$	Ni–$Fe_{3.33}Ni_{8.67}$–$Fe_{0.43}Ni_{1.57}$	Fe–$Ni_{3.33}Fe_{8.67}$–$Ni_{0.43}Fe_{1.57}$	$[Ni–Ni_{8.3}Fe_{3.7}]Ni_2$	$[Fe–Fe_{0.7}Ni_{11.3}]Fe_2$	$[Fe–Ni_8Fe_4]Fe_2$ + $[Ni–Ni_{12}]Ni_2$	76.9	0.3
75[27]	$\alpha_{110} = -0.1305$ $\alpha_{200} = 0.1388$	Ni–$Fe_{3.39}Ni_{8.61}$–$Fe_{0.43}Ni_{1.57}$	Fe–$Ni_{3.39}Fe_{8.61}$–$Ni_{0.43}Fe_{1.57}$					
76.5[29]	$\alpha_{110} = -0.0868$ $\alpha_{200} = 0.1005$	Ni–$Fe_{3.06}Ni_{8.94}$–$Fe_{0.42}Ni_{1.58}$	Fe–$Ni_{3.06}Fe_{8.94}$–$Ni_{0.42}Fe_{1.58}$	$[Ni–Fe_{3.5}Ni_{8.5}]Ni_2$	$[Fe–Fe_{0.5}Ni_{11.5}]Fe_2$			0.2
77.5[29]	$\alpha_{110} = -0.10821$ $\alpha_{200} = 0.11948$	Ni–Fe_3Ni_9–$Fe_{0.4}Ni_{1.6}$	Fe–Ni_3Fe_9–$Ni_{0.4}Fe_{1.6}$	$[Ni–Fe_{3.4}Ni_{8.6}]Ni_2$	$[Fe–Fe_{0.4}Ni_{11.6}]Fe_2$			0.1
77.5[27]	$\alpha_{110} = -0.13664$ $\alpha_{200} = 0.12729$	Ni–$Fe_{3.01}Ni_{8.93}$–$Fe_{0.39}Ni_{1.61}$						

3 Electronic Model Analysis of Fe–Ni Alloys with Constant Expansion

3.1 Spherical periodic electronic resonant range in fcc solid solution alloys

When the short range of fcc solid solution alloys participating in the Friedel spherical periodic resonance is determined, the numbers of first nearest-neighbor clusters and second nearest-neighbor atoms that are packed between these clusters within the resonant range are evaluated. In this section, the resonant range of stable short-range ordered structures is obtained. Then, the chemical structure formula of the model is concluded to be $[X–Y_{12}]Z_2$, where X, Y, and Z are the composited atoms in the alloy.

There is an inheritance of the short-range ordered structure among liquid metals, amorphous alloys, and the ordered solid solutions.(31) On the basis of the principle of structural stability corresponding to the lowest energy, whether in amorphous or solid solution alloys, the distribution of electrons is consistent.

Häussler verified that when the maximum atomic distribution corresponds to the minimum effective pair potential energy in molten or amorphous alloys, the energy possessed by the energy band structure is minimal.(32) This causes the entire system to have the lowest energy and the most stable structure.

When there are defects such as impurities or solute atoms in the bulk alloy, to obtain electric neutrality, the electrons are rearranged to shield the bulk alloy from the effect of impurity charges. The distribution of electronic density centered on the impurities exhibits the form of long-range attenuation resonance. This resonance only exists within the range of a few atoms.

The oscillation of the electronic density around the ionic atom, which is an impurity atom as stated above, is called Friedel oscillation (FO). This oscillation forces the electrons to be located at different concentric spheres centered on the ion atom.(32)

FO is a result of the resonance of electrons and atoms in the gap position with the lowest energy and the most stable structure. For the fcc solid solution alloys, the key point is to determine the range or number of atoms involved in FO.

The effective pair potential energy $\phi_{eff}(r)$ for the electrons at distance r from the central ion atom is(32)

$$\phi_{eff}(r) \propto \cos(2k_F r + \Theta)/r^3, \tag{1}$$

where k_F is the Fermi radius of the distribution of electrons in the wave vector space and Θ is the phase offset. Experiments show that the phase offset is $\Theta = \pi/2$ in the liquid metals and amorphous alloys with short- or medium-range orders.(32)

In real space, the band structure energy U_{bs} is given as

$$U_{bs} \propto \int [g(r)-1]\phi_{eff}(r) r^2 dr, \tag{2}$$

when the effective pair potential energy $\phi_{eff}(r)$ of the electrons is at the local minimum, i.e., when the atomic density $g(r)$ is at the local minimum, U_{bs} is minimum. This indicates that the

ion is bound by FO at the local minima of $\phi_{eff}(r)$. The stable phase is formed when metal phase transition occurs.[32]

The position of the local minimum for $\phi_{eff}(r)$ is obtained as

$$r_n = (1/4 + n)\lambda_{Fr}, n = 1, 2, \cdots, \tag{3}$$

where $\lambda_{Fr} = 2\pi/2k_F$ is the Friedel wavelength[32] and r_n is the position of the nth-shell neighbor atoms around the central ion atom.

Compared with the structure of liquid alloys, the solid solutions have the same stable structure as FO for the local-range atoms. Truncated octahedral clusters (TOCs) are located not only at the points of the sphere determined by FO but also at the points of the lattice determined by the fcc structure, as shown in Fig. 1.

Figure 1 shows the distribution of the nearest two shell atoms. The TOC is formed by the first nearest atoms, and the yellow atoms are the second nearest atoms of the central atom of the TOC. If the central atom of one TOC, which is the big red atom in Fig. 1, is located at the origin, then its shell atoms are located at a distance of $r_1 = 1.25\lambda_{Fr}$ from the origin. The central atoms of the TOCs adjacent to the TOC at the origin, which are the big blue atoms in Fig. 1, are located at a distance of $r_3 = 3.25\lambda_{Fr}$, and their nearest atoms are located at a distance of $r_2 = 2.25\lambda_{Fr}$ or from the origin.

The red curve for the effective pair potential energy of the electrons, $\phi_{eff}(r)$, is also shown in Fig. 1. It tends to zero with increasing distance $r_n(\lambda_{Fr})$. This means that the short-range ordered structure determined from FO is reduced to zero when r exceeds $r_4 = 4.25\lambda_{Fr}$.

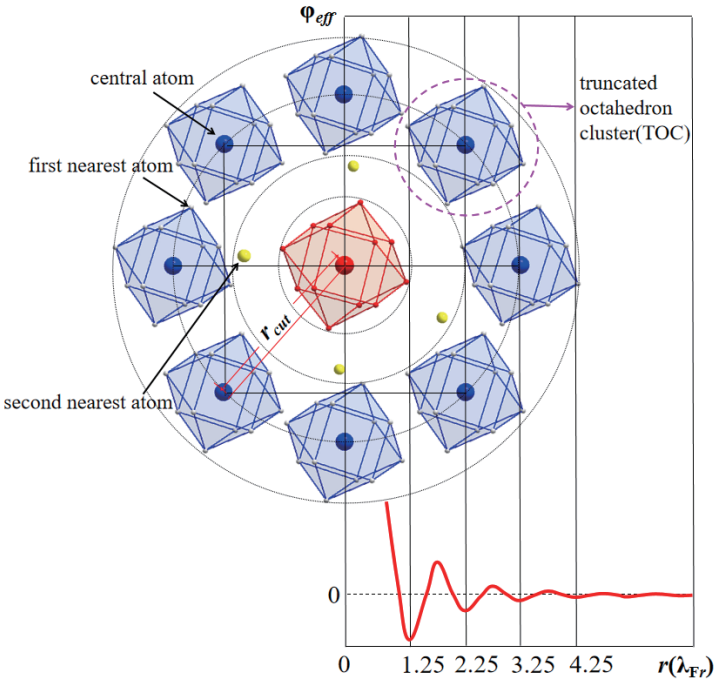

Fig. 1. (Color online) Spherical periodic short-range ordered structure.

In three-dimensional space, a TOC has a strong interaction with its adjacent TOC. Electronic resonance is achieved through momentum exchange between the electrons and the ions within the range of FO.[32]

When one layer of atoms slides relative to its neighbor layer of atoms, the slip is significantly resisted by the FO structure. That is, the FO structure is sufficiently stable to prevent further sliding. Therefore, the resistance to plastic deformation increases the strength as well as the hardness of the alloys.

There are a few packed atoms (PAs) between adjacent TOCs. The number of PAs, n, within the FO range depends on the number of clusters in this range and the size of this range. The structure of the TOCs and PAs is expressed by the chemical formula $[X–Y_{12}]–Z_n$, where $[X–Y_{12}]$ is the cluster formed by the central atom of the nearest shell. X is the central atom of the TOC, Y_{12} are the 12 nearest atoms in the structure of a truncated octahedron, and Z_n (n is an integer) are the second shell Z atoms.

3.2 First and second nearest-neighbor atomic models in fcc solid solution alloys

In fcc solid solutions, the key point in determining the chemical formula is the location of the TOCs, which are located at the positions determined by the FO and fcc lattice structures.

In this study, one position for TOCs in the fcc alloy is introduced in Fig. 2. In Fig. 2(a), the fcc lattice structure, lattice constant a, and TOCs are depicted. In Fig. 2(b), the parallelepiped, one

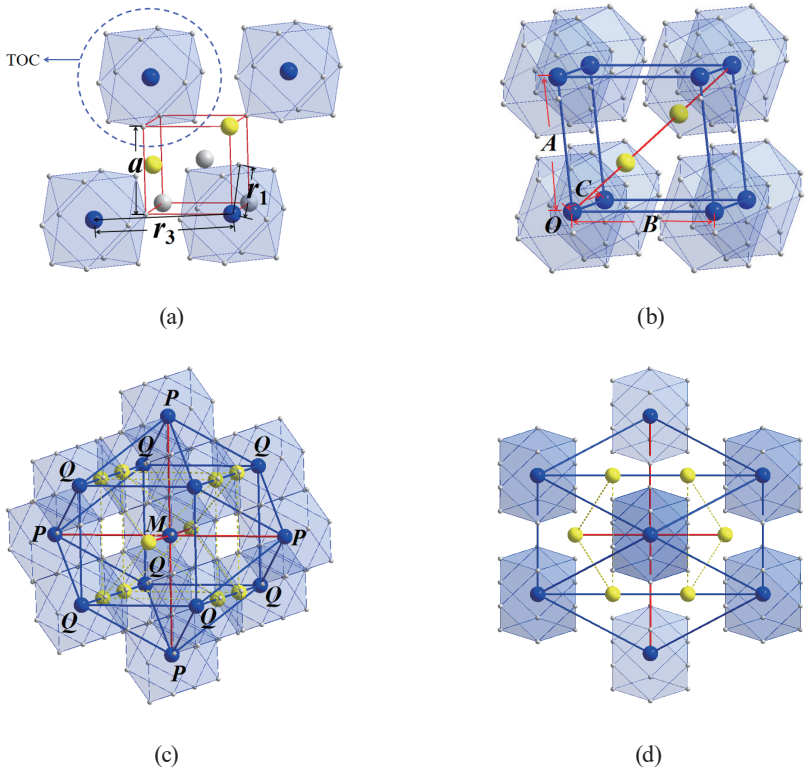

Fig. 2. (Color online) Structural models of clusters for fcc alloys.

TOC's unit cell formed by eight TOCs, which is called the unicell of a TOC (UCTOC), is shown. Its CSF is $[X–Y_{12}]Z_2$. The ratio of the number of TOCs to that of PAs is 1:2. In Fig. 2(c), a midrange structure through outward growth from the unicell is called the super unicell of a TOC (SUCTOC) and has the quadrilateral axis symmetry. Figure 2(d) shows the structure in Fig. 2(c) from another perspective. It has the hexagonal axis symmetry.

In Fig. 2(a), for the fcc alloy, the distance between the shell atoms on the TOC and the origin is $r_1 = 1.25\lambda_{Fr}$. Moreover, $r_1 = a/\sqrt{2} \approx 0.707a$, where a is the fcc lattice constant. The central atom of the TOC closest to the origin is located at r_3, which, in accordance with Eq. (3), is evaluated as

$$r_3 = \left(\frac{1}{4}+3\right)\lambda_{Fr} = \frac{13}{4}\times\frac{r_1}{1.25} = \frac{13}{5}\times\frac{a}{\sqrt{2}} \approx 1.838a. \tag{4}$$

Eighteen different types of unicell model are evaluated for the fcc solid solution using Matlab.[33] Their CSF is expressed as $[X–Y_{12}]\ –Z_n$, where n is the number of PAs.

When $n = 2$, that is, the TOC:PA ratio is 2, the model is called 2–2 and is shown in Fig. 2(b). One TOC is at $O(0,0,0)$ and there are three TOCS at $\vec{A} = \frac{1}{2}(-3,-1,0)$, $\vec{B} = \frac{1}{2}(-2,2,-2)$, and $\vec{C} = \frac{1}{2}(0,-1,-3)$. The parallelepiped unicell is composed of these four TOCs as the basic vector, as shown in Fig. 2(b). The polyhedral structure is obtained by growing the unicell outward in a planar periodic sequence, as shown in Fig. 2(c). There are four TOCs in the first nearest shell. Their central point P is at a distance of $1.581a$ from the central TOC at point M. There are eight TOCs in the second nearest shell. Then, their central point Q is at a distance of $1.8701a$ from point M.

The average distance between the central point P or Q of the 12 TOCs and point M is obtained as

$$\bar{R} = \frac{1}{n}\sum_{k=1}^{n} R_k = (1.8701a\times 8 + 1.581a\times 4)/12 = 1.774a, \tag{5}$$

where R_k is the position of the kth cluster and n is the total number of clusters. Then, the deviation between $\bar{R}$ and the third position of FO, $r_3 \approx 1.838a$, is $\Delta = |r_3 - \bar{R}| = 0.064a$. The lattice constant of iron is $a = 2.86 \times 10^{-10}$ min an iron-based alloy. Then, the deviation is $\Delta = 1.83 \times 10^{-11}$ m. The ratio of the deviation Δ to the radius of the iron atom, $r_{Fe} = 1.241 \times 10^{-10}$, is $\Delta/r_{Fe} = 0.147$.

There are three layers of atoms within the distance of r_3, so the deviation Δ is the difference shared by three atoms. The average deviated distance of each atom from their original position is $0.07r_{Fe}$. This is close to the amplitude of the thermal vibration of the atom on the lattice position, indicating that the atoms do not truly deviate from the original lattice positions but merely undergo thermal motion at their original positions. The 2–2 model provides the exact range for r_3 in the fcc solid solution in accordance with the theorical value $r_3 = 3.25\lambda_{Fr}$ determined using the FO structure. The model also has high symmetry, as shown in Figs. 2(c) and 2(d).

The deviation Δ and volume density ρ for the 18 different types of model reported in Ref. 33 are evaluated by the aforementioned calculation procedure and shown in Fig. 3. The volume density is defined as

$$\rho = \left(\text{Number of atoms in the cut shell}\right) / r_{cut}^3 , \tag{6}$$

where $r_{cut} = r_3$ is the radius of the cut shell, as shown in Fig. 1. In Fig. 3, it is observed that there are five suitable candidate models, that is, 2–2, 3–1, 4–2, 5–5, and 6–3, with relatively small deviation Δ = −0.0639, 0.0086, −0.0531, −0.0398, −0.0398 and high volume density ρ = 26.57, 21.99, 24.74, 21.38, 22.9 values, respectively. This means that the thermal vibrations of the atoms within the FO structure all occur near the lattice positions in these five atomic models.

Because metal bonds have no directivity or saturation, the atoms in fcc alloys tend to be arranged with higher bulk density ρ values. The atomic volume density is higher and the potential energy of the alloy is lower. They lead to a more stable alloy structure. The 2–2 model has the highest bulk density ρ and a petty deviation Δ among the 18 models reported in Ref. 33, as shown in Fig. 3. This means that the structure of the 2–2 SUCTOCs has the excellent stability to meet the conditions of both FO and the highest bulk density. The CSF of the structure is expressed as $[X–Y_{12}]$ $–Z_2$, where 2 is the number of PAs. This formula can be verified by the explanation of Fe–Ni alloy grades in the next section.

4 Electronic Model Analysis of Fe–Ni-based Constant-expansion Alloy and Discussion

Because their coefficient of thermal expansion matches that of many sealing materials, Fe–Ni alloys are often used as sealing materials. The Ni content of these alloys ranges from 42 to 54 wt.%. The common characteristics of these alloys are good plasticity, electrical and thermal

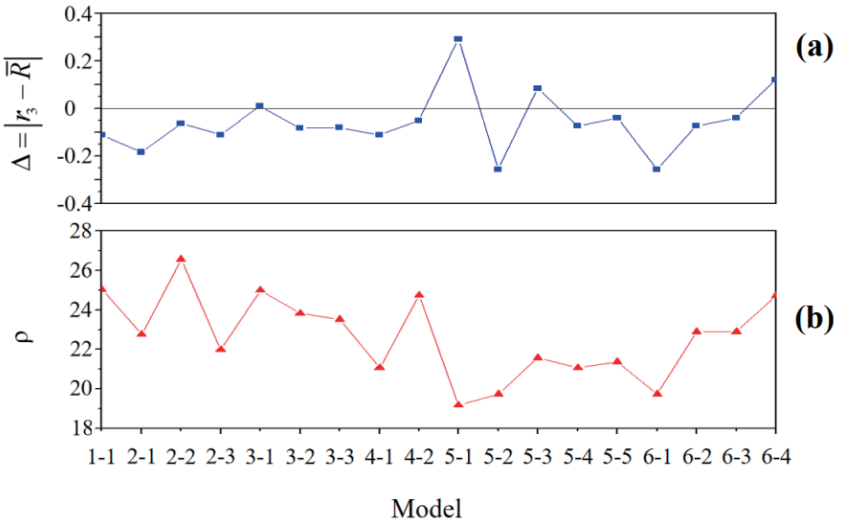

Fig. 3. (Color online) Deviation Δ and volume density ρ values of atomic models.

conductivity, and processability. In addition, the key point is that these materials remain in the original γ phase during storage and working.[34] They do not undergo phase transition, which means that their stability is extremely high.

In the following, the 2–2 model with the analysis steps introduced in Sect. 3 is applied to analyze the Fe–Ni-based constant-expansion alloys. The results are listed in Table 3, where the wt.% is the abbreviation for the weight percentage of Ni in Fe–Ni alloys. The Fe–Ni alloys listed in Table 3 can be analyzed using the formula $[X–Y_{12}]Z_2$ of the 2–2 model. The chemical compositions of the elements in the formula are basically consistent with those specified by the manufacturer. From the results in Table 3, the following is concluded.

(1) The composition of 42–54 Ni wt.% Fe–Ni sealing alloys was analyzed using $[X–Y_{12}]Z_2$, where Y is the combination of Fe and Ni atoms and Z is the Fe or Ni atom. The total number of atoms was 15. The composition formula for these binary alloys was in the range of Ni_6Fe_9 to Ni_8Fe_7.
   (I) Two components were analyzed using the single cluster model. The CSFs were $[Ni–Fe_8Ni_4]Ni_2$ (47.9 wt.%) and $[Fe–Ni_8Fe_4]Fe_2$ (54.5 wt.%).
   (II) Three components were analyzed using the double cluster model. The CSFs were $[Fe–Ni_8Fe_4]Fe_2 + [Fe–Fe_8Ni_4]Fe_2$ (41.2 wt.%), $[Fe–Ni_8Fe_4]Fe_2 + [Ni–Ni_4Fe_8]Fe_2$ (44.6 wt.%), and $[Fe–Ni_8Fe_4]Fe_2 + [Ni–Fe_8Ni_4]Ni_2$(51.3 wt.%).

Table 3
Cluster formulas and properties of Fe–Ni alloys.

Specification	Range of specification Ni wt.%*	Chemical formula	Component formula for 15 atoms	Ni wt.% in chemical formula	Bi-cluster chemical formula	Ni wt.% in bicluster chemical formula
Ni_{42}	41.5–42.5	**$[Fe–Ni_6Fe_6]Fe_2$**	Fe_9Ni_6	41.2	**$[Fe–Ni_8Fe_4]Fe_2$** **$[Fe–Fe_8Ni_4]Fe_2$**	41.2
Ni_{43}	42.5–43.5	$[Fe–Ni_{6.27}Fe_{5.73}]Fe_2$	$Fe_{8.73}Ni_{6.27}$	43	**$[Fe–Ni_8Fe_4]Fe_2$** **$[Fe–Fe_8Ni_4]Fe_{1.5}Ni_{0.5}$**	42.9
Ni_{45}	44.5–45.5	$[Fe–Ni_{6.57}Fe_{5.43}]Fe_2$	$Fe_{8.43}Ni_{6.57}$	45	**$[Fe–Ni_8Fe_4]Fe_2$** **$[Ni–Ni_4Fe_8]Fe_2$**	44.6
Ni_{48}	47–48	**$[Ni–Fe_8Ni_4]Ni_2$**	Fe_8Ni_7	47.9	—	
Ni_{50}	49.5–50.5	$[Fe–Ni_{7.31}Fe_{4.69}]Fe_2$	$Fe_{7.69}Ni_{7.31}$	50	**$[Fe–Ni_8Fe_4]Fe_2$** **$[Ni–Fe_8Ni_4]Ni_2$**	51.3
Ni_{52}	51.5–52.5	$[Fe–Ni_{7.61}Fe_{4.39}]Fe_2$	$Fe_{7.39}Ni_{7.61}$	52		
Ni_{54}	53.5–54.5	**$[Fe–Ni_8Fe_4]Fe_2$**	Fe_7Ni_8	54.5	—	
$Ni_{42}Cr_6$	41.5–42.5 5.5–6.3 rem	**$[Cr–Ni_6Fe_6]Fe_2$**	—	Ni: 41.4 Cr: 6.1 Fe: rem	**$[Fe–Fe_8Ni_4]Cr_2$** **$[Fe–Ni_8Fe_4]Fe_2$**	Ni: 41.4 Cr: 6.1 Fe: rem
$Ni_{47}Cr_5$	46–48 5–6 rem	**$[Ni–(Fe_7Cr)Ni_4]Ni_2$**	—	Ni: 48.1 Cr: 6.1 Fe: rem	—	
$Ni_{29}Co_{18}$	28.5–29.5 16.8–17.8 rem	$[Co–Fe_{8.5}(Co_{1.5}Ni_2)]Ni_2$	—	Ni: 27.4 Co: 17.2 Fe: rem	**$[Fe–Fe_8Ni_4]Ni_2$** **$[Co–Co_4Fe_8]Ni_2$**	Ni: 27.4 Co: 17.2 Fe: rem
$Ni_{33}Co_{14}$	32.5–34 13.6–14.8 rem	**$[Ni–Fe_8Ni_4]Co_2$**	—	Ni: 34.2 Co: 13.7 Fe: rem	—	
$Ni_{29}Co_{20}$	28.5–29.5 19.5–20.5 rem	**$[Co–Fe_8Ni_4]Co_2$**	—	Ni: 27.4 Co: 20.6 Fe: rem	—	

(III) There was another component that could not be resolved into an integer ratio cluster expression. Its two-cluster CSFs were $[Fe–Ni_8Fe_4]Fe_2 + [Fe–Fe_8Ni_4]Fe_{1.5}Ni_{0.5}$.

(IV) There were three types of TOC in the first neighbor clusters for all Fe–Ni sealing alloys, namely, $[Fe–Ni_8Fe_4]$, $[Ni–Fe_8Ni_4]$, and $[Fe–Fe_8Ni_4]$, which were derived from the ordered phases of FeNi and $FeNi_3$, as shown in Table 1.

(V) The number of atoms in the second shell of the structural formulas was 2 in all cases. It was proven that the 2–2 model has the highest compactness of the fcc solid solution.

(2) For the analysis of the ternary Fe–Ni sealing alloys, the results are summarized for the nickel–chromium–iron alloys with $Ni_{42}Cr_6$ and $Ni_{47}Cr_5$ in sequence.

(I) The CSFs were $[Fe–Fe_8Ni_4]Cr_2 + [Fe–Ni_8Fe_4]Fe_2$ and $[Ni–(Fe_7Cr)Ni_4]Ni_2$.

(II) The double-cluster CSF of the $Ni_{42}Cr_6$ alloy, $[Fe–Fe_8Ni_4]Cr_2 + [Fe–Ni_8Fe_4]Fe_2$, was obtained by replacing the second shell atom in the first CSF of $[Fe–Fe_8Ni_4]Fe_2 + [Fe–Ni_8Fe_4]Fe_2$ with a Cr atom in the first CSF of $[Fe–Fe_8Ni_4]Fe_2$.

(III) Similarly, the CSF of the $Ni_{47}Cr_5$ alloy, $[Ni–(Fe_7Cr)Ni_4]Ni_2$, was obtained by replacing an Fe atom in the nearest-neighbor shell of $[Ni–Fe_8Ni_4]Ni_2$ in the CSF of the Ni–48 alloy with a Cr atom.

(IV) The above results are consistent with the mixing enthalpy of the alloys, wherein $\Delta H_{Fe–Ni} = -2$ KJ/mol, $\Delta H_{Cr–Ni} = -7$ KJ/mol, and $\Delta H_{Fe–Cr} = -1$ KJ/mol.[35] The mixing enthalpy reflects the dispersion and mixing degree of atoms in the system, and the absolute values of the mixing enthalpy of Fe and Cr atoms are the smallest. This means that these two atoms have the least force and can be substituted.

(3) The results are summarized for the iron–nickel–cobalt alloys with $Ni_{33}Co_{14}$, $Ni_{29}Co_{20}$, and $Ni_{29}Co_{18}$ as follows.

(I) The CSFs of such alloys were $[Ni–Fe_8Ni_4]Co_2$, $[Co–Fe_8Ni_4]Co_2$, and $[Fe–Fe_8Ni_4]Ni_2 + [Co–Fe_8]Co_4Ni_2$, respectively.

(II) The CSFs of the $Ni_{33}Co_{14}$ and $Ni_{29}Co_{20}$ alloys were obtained by replacing the Ni atom with the Co atom in the CSF of the Ni48 alloy, $[Ni–Fe_8Ni_4]Ni_2$.

(III) The CSF of the $Ni_{29}Co_{18}$ alloy was obtained by replacing five Ni atoms with five Co atoms in the double-cluster CSF of $[Fe–Fe_8Ni_4]Ni_2 + [Co–Fe_8]Co_4Ni_2$.

(IV) The above CSFs are consistent with the mixing enthalpy of the alloys, wherein $\Delta H_{Fe–Ni} = -2$ KJ/mol, $\Delta H_{Co–Ni} = -0$ KJ/mol, and $\Delta H_{Fe–Co} = -1$ KJ/mol.[35] Because the mixing enthalpy of Co and Ni atoms is zero, the two atoms are interchangeable in structural formulas of the iron–nickel–cobalt alloys.

In the aforementioned structural formulas of the Fe–Ni sealing alloys, the atoms in the first shell are different from the central atom, and the atoms in the second shell are of the same type as the central atom.

The structural formula of the 2–2 model for the nearest two-shell atoms, which is obtained from the spherical periodic ordered model, is basically consistent with the relationship between the attractive and repulsive forces determined by the mixing enthalpy of atoms. In Table 3, the analyzed components of common Fe–Ni sealing alloys basically fall into the composition ranges of the alloys specified by the manufacturer. Only a few values for the alloys are slightly off, which are underlined. It is further proved that the 2–2 model developed from the spherical

periodic ordered model, which is described in Sect. 3, can be used to analyze all the Fe–Ni sealing alloys.

Because there is no long-range order in the disordered solid solution alloy, the short-range ordered structure only exists in a small range of FO. The heterogeneous clusters different from the TOCs, such as holes, dislocations, and interstitial sites, prevent the growth of the short-range ordered structure. Therefore, it is not easy to form the long-range ordered chemical structures of whole crystals.

The fcc alloy compositions obtained by similar procedures have been reported.[36–39] For example, the Cu–Ni–Si ternary alloys were analyzed by selecting the nearest-neighbor clusters from the precipitated and strengthened phases.[36,37] The number of second nearest-neighbor atoms was directly assigned the value of 1 or 3 without proposing any assignment principles. The binary copper alloy was analyzed by selecting the nearest-neighbor cluster from Cowley parameters and determining the number of second nearest-neighbor atoms from the empirical values of amorphous alloys and the density of the densest stacked crystal structure.[38,39] In this study, the determination and selection of the number of nearest second-shell atoms are based on the ordered phases, Cowley parameters, the maximum bulk density of atoms, and FO. Compared with the previously obtained results,[36–39] the proposed methods can enhance the reliability of the analysis of alloy compositions.

5. Conclusions

In the study, the tools for analyzing metal alloys, such as Cowley parameters, FO, and the NNTS atomic model, were addressed. They were also applied to analyze Fe–Ni binary or even ternary sealing alloys successfully. The conclusions of the work are shown below.

(1) The chemical composition formula of the NNTS model was inferred from $[X–Y_{12}]Z_n$ where n is an integer. $X–Y_{12}$ is composed of the first nearest–neighbor shell atoms. The combinations $Ni–Ni_8Fe_4$, $Fe–Ni_{12}$, $Ni–Fe_8Ni_4$, $Fe–Ni_8Fe_4$, $Ni–Fe_{12}$, and $Fe–Fe_8Ni_4$ are included in $X–Y_{12}$.
(2) Various Fe–Ni alloys with nickel contents in the range of 30 to 80 at.% were analyzed using one or two types of $[X–Y_{12}]Z_2$ model. The results were consistent with those calculated using Cowley parameters.
(3) Compared with the most stable structure of the alloy, it was pointed out that the 2–2 model is the most stable structure in the fcc solid solution. The atomic density of the 2–2 model is the highest in the short range of the Friedel spherical periodic resonance structure.
(4) Both Fe–Ni binary and ternary alloys were analyzed using two types of $[X–Y_{12}]Z_2$ model. Our results revealed an effective approach for the composition design of alloys.

Acknowledgments

This work was supported in part by Projects for the Department of Science and Technology of Fujian Province (Grant nos. 2020-H-0049, 2021-H-0060, and 2021-G-02013), the Operational Funding of the Advanced Talents for Scientific Research (Grant nos. 19YG04 and 19YG05) of Sanming University, and the Natural Science Foundation of Sanming University (Grant no. 113/

A160002). The authors also acknowledge the support from the School of Mechanical and Electric Engineering, Sanming University.

References

1 P. Edinger, G. Jo, C. P. Van Nguyen, A. Y. Takabayashi, C. Errando-Herranz, C. Antony, and K. B. Gylfason: Opt. Express **31** (2023) 6540. https://doi.org/10.1364/OE.480219
2 S. S. K. Ardestani, V. Dashtizad, and A. Kaflou: Ceram. Int. **47** (2021) 2008. https://doi.org/10.1016/j.ceramint.2020.09.032
3 M. Jing, G. Ni, C. Zhu, Z. Li, G. Wang, Z. Wang, and Q. Huang: Constr. Build. Mater. **377** (2023) 131076. https://doi.org/10.1016/j.conbuildmat.2023.131076
4 P. Yu, F. Zhan, W. Rao, Y. Zhao, Z. Fang, Z. Tu, Z. Li, D. Guo, and X. Wei: Micromachines. **14** (2023) 84. https://doi.org/10.3390/mi14010084
5 M. Wei, F. He, X. Cao, B. Zhang, C. Zheng, and J. Xie: Ceram. Int. **48** (2022) 27718. https://doi.org/10.1016/j.ceramint.2022.06.072
6 M. M. Uddin, J. Jie, C. Wang ,C. Zhang, and W. Ke: Energy Build. **286** (2023) 112939. https://doi.org/10.1016/j.enbuild.2023.112939
7 Q. Sun, G. Sun, Y. Liu, H. Chen, M. Li, C. Huang, and W. Zhu: J. Mater. Sci-Mater. El. **32** (2021) 16230. https://doi.org/10.1007/s10854-021-06171-3
8 D. M. Chen, L. F. Hu, Y. Z. Xue, S. Chen, and W. Wang: Trans. China Weld. Inst. **39** (2018) 71. https://doi.org/10.12073/j.hjxb.2018390227
9 Q. Lu,W. Li, X. Zhang, Z. Liu, Q. Cao, X. Xie, and S. Yan: Fuel **263** (2020) 116690. https://doi.org/10.1016/j.fuel.2019.116690
10 H. L. Hong, C. H. Yang, K. C. Wang, and H. X. Yan: Mod. Phys. Lett. B **35** (2021) 2141009. https://doi.org/10.1142/S0217984921410098
11 I. Y. Khairani, Q. Lin, J. Landers, S. Salamon, C. D. Buendia, E. Karapetrova, H. Wendi, G. Zangari, and B. Gökce: Nanomaterials **13** (2023) 227. https://doi.org/10.3390/nano13020227
12 Y. Wu, F. Zhang, X. Yan, H. Huang, X. Wen, Y. Wang, M. Zhang, H. Wu, X. Liu, and H. Wang: J. Mater. Sci. Technol. **62** (2021) 214. https://doi.org/10.1016/j.jmst.2020.06.018
13 F. D. C. Garcia Filho, R. O. Ritchie, M. A. Meyers, and S. N. Monteiro: J. Mater. Res. Technol. **17** (2022) 1868. https://doi.org/10.1016/j.jmrt.2022.01.118
14 S. Bao, X. W. Guo, Z. L. Wang, Q. Zhao, Y. L. Liu, F. S. Meng, B. Z. Sun, N. Jia, and Y. Qi: Scripta Mater. **224** (2023) 115132. https://doi.org/10.1016/j.scriptamat.2022.115132
15 Y. Liu, J. Luo, and X. Huang: J. Alloy. Compd. **932** (2023) 167591. https://doi.org/10.1016/j.jallcom.2022.167591
16 Y. Li, D. Yang, and W. Qiang: J. Alloy. Compd. **931** (2023): 167588. https://doi.org/10.1016/j.jallcom.2022.167588
17 D. He, G. Liu, J. Liu, H. Xie, D. Yue, Z. Chen, C. Wei, X. Xu, and H. Xie: Corros. Sci. **211** (2023) 110917. https://doi.org/10.1016/j.corsci.2022.110917
18 A. Abu-Odeh, and M. Asta: Acta Mater. **226** (2022) 117615. https://doi.org/10.1016/j.actamat.2021.117615
19 R. Ma, J. Rong, S. Zhang, H. Wang, and G. Yun: J. Phys. Soc. Jpn. **89** (2020) 044705. https://doi.org/10.7566/JPSJ.89.044705
20 A. Toriyabe, W. T. Chiu, A. Umise, M. Tahara, K. Goto, H. Kanetaka, T. Hanawa, and H. Hosoda: Intermetallics. **139** (2021) 107349. https://doi.org/10.1016/j.intermet.2021.107349
21 S. Jiang, F. Zhou, W. Liu, S. Liu, X. Wang, S. Zhang, X. Zhu, R. Wei, P. Zheng, and Z. Lin: Fusion Eng. Des. **193** (2023) 113658. https://doi.org/10.1016/j.fusengdes.2023.113658
22 D. D. Johnson, J. D. Althoff, F. J. Pinski, J. B. Staunton, and M. F. Ling: J. Phase Equilib. **18** (1997) 598. https://doi.org/10.1007/BF02665818
23 J. S. Wróbel, D. Nguyen-Manh, Y. M. Lavrentiev, M. Marek, and S. L. Dudarev: Phys. Rev. B, **91** (2015) 024108. https://doi.org/10.1103/PhysRevB.91.024108
24 D Gehringer, M Friák, and D Holec: Comput. Phys. Commun. **286** (2023) 108664. https://doi.org/10.1016/j.cpc.2023.108664
25 X. Jiang, G. E. Ice, C. J. Sparks, L. Robertson, and P. Zschack: Phys. Rev. B. Condens Matter. **4** (1996) 3211. https://doi.org/10.1103/PhysRevB.54.3211
26 P. Cenedese, F. Bley, and S. Lefebvre: Mater. Sci. **21** (1983) 351. https://doi.org/10.1557/PROC-21-351
27 S. M. Bokoch, V. A. Tatarenko, and I. V. Vernyhora: Usp. Fiz. Met. **13** (2012) 269. http://dspace.nbuv.gov.ua/handle/123456789/98336
28 J. L. Robertson, G. E. Ice, C. J. Sparks, X. Jiang, P. Zschack, F. Bley, S. Lefebvre, and M. Bessiere: Phys. Rev. Lett. **82** (1999) 2911. https://doi.org/10.1103/PhysRevLett.82.2911

29 G. E. Ice, C. J. Sparks, A. Habenschuss, and L. B. Shaffe: Phys. Rev. Lett. **68** (1992) 863. https://doi.org/10.1103/PhysRevLett.68.863
30 S. Lefebvre, F. Bley, M. Fayard, and M. Roth: Acta Metall. **29** (1981) 749. https://doi.org/10.1016/0001-6160(81)90118-8
31 L. Zhang, S. Su, W. Fu, J. Sun, Z. Ning, A. H. W. Ngan, and Y. Huang: Compos. Part B: Eng. **258** (2023) 110698. https://doi.org/10.1016/j.compositesb.2023.110698
32 P. Häussler: J. Phys. Colloques. **46** (1985) 361. https://doi.org/10.1051/jphyscol:1985854
33 H. L. Hong, C. Dong, and Y. Zhang: Acta Phys. Sin. **65** (2016) 036101. https://wulixb.iphy.ac.cn/article/doi/10.7498/aps.65.036101
34 W. Liu, C. Chen, Y. Tang, Q. Long, S. Wei, G. Zhang, F. Mao, Q. Jiang, T. Zhang, and M. Liu: Calphad. **69** (2020) 101763. https://doi.org/10.1016/j.calphad.2020.101763
35 A. Takeuchi, and A. Inoue: Mater. Trans. **46** (2005) 2817. https://doi.org/10.2320/matertrans.46.2817
36 D. M. Li, J. Y. Han, and C. Dong: Acta Phys. Sin. **68** (2019) 196102. https://doi.org/10.7498/aps.68.20190593
37 D. M. Li, Q. Wang, B. B. Jiang, X. X. Li, W. L. Zhou, C. Dong, H. Wang, and Q. X. Chen: Prog. Nat. Sci.: Mater. Int. **27** (2017) 467. https://doi.org/10.1016/j.pnsc.2017.06.006
38 Z. Li, D. D. Dong, L. Zhang, S. Zhang, Q. Wang and C. Dong: Sci. Rep. **12** (2022) 3169. https://doi.org/10.1038/s41598-022-06893-2
39 C. Dong, D. D. Dong, and Q. Wang: Acta Metall. Sin. **54** (2018) 293. https://www.ams.org.cn/CN/10.11900/0412.1961.2017.00462